FULL PAPER

Tumor Treatment

ADVANCED
HEALTHCARE
MATERIALS

www.advhealthmat.de

pH-Responsive Nanoscale Coordination Polymer for Efficient Drug Delivery and Real-Time Release Monitoring

Kai Han,* Wei-Yun Zhang, Jin Zhang, Zhao-Yu Ma, and He-You Han*

Both excess dosages of drug and unwanted drug carrier can lead to severe side effects as well as the failure of tumor therapy. Here, an Fe^{3+}–gallic acid based drug delivery system is designed for efficient monitoring of drug release in tumor. Fe^{3+} and polyphenol gallic acid can form polygonal nanoscale coordination polymer in aqueous solution, which exhibits certain antitumor effect. Importantly, this coordination polymer possesses extremely high doxorubicin (DOX) loading efficacy (up to 48.3%). In vitro studies demonstrate that the fluorescence of DOX can be quenched efficiently when DOX is loaded on the coordination polymer. The acidity in lysosome also triggers the release of DOX and fluorescence recovery simultaneously, which realizes real-time monitoring of drug release in tumor cells. In vivo studies further indicate that this polyphenol-rich drug delivery system can significantly inhibit tumor growth with negligible heart toxicity of DOX. This system with minimal side effects should be a promising nanoplatform for tumor treatment.

1. Introduction

Fabrication of novel drug delivery systems (DDSs) with high therapeutic efficacy and negligible side effects has obtained substantial research interest during last decades.[1–4] Although various DDSs have been developed to alter the pharmacokinetics and biodistribution of drugs, only drug itself is a therapeutically relevant compound in traditional DDSs, and the drug carriers are just excipients for drug delivery.[5–7] Even worse, these carriers always have unsatisfied drug loading efficacy. As a result, high dosages of unwanted carriers are required to ensure the clinical therapeutic efficacy, leading to poor elimination and severely systemic toxicity inevitably.[8,9] To overcome this dilemma, construction of drug delivery systems with high dosages and the carriers that also have therapeutical effect has been proposed.[10,11] For example, Zhang and co-workers fabricated a photosensitizer/proapoptosis peptide self-delivery system with mitochondria in situ photodynamic therapy.[12] Yan and co-workers constructed drug–drug conjugation with efficient antitumor therapy in both in vitro and in vivo.[13]

Dr. K. Han, W.-Y. Zhang, J. Zhang, Z.-Y. Ma, Prof. H.-Y. Han
State Key Laboratory of Agricultural Microbiology
College of Science
Huazhong Agricultural University
Wuhan 430070, China
E-mail: hank@mail.hzau.edu.cn; hyhan@mail.hzau.edu.cn

Hashida and co-workers developed carrier-free pure nanodrugs via a simple reprecipitation method.[14] Great success has been achieved in these delivery systems, especially in improving drug loading efficacy. However, the clinical trials of these systems are still hampered. Since drugs are usually linked in these systems via biodegradable covalent bonds, the concentration of free drugs in targeted cells is actually uncertain, which will lead to repeated doses or inappropriate therapy.

Although real-time monitoring of drug release in targeted cells exhibits great potential to overcome this hurdle,[15,16] current monitoring of drug release is always studied via a typical dialysis model in vitro to simulate the intracellular environment.[17] Real-time monitoring of drug release inside targeted cells is severely ignored in most of DDSs, partly because of the challenging of design efficient strategy to realize it. The most prevalent strategy includes using nuclear techniques such as single-photon emission computed tomography and positron emission tomography[18] or employing fluorescent dyes to simulate drugs.[19] Nuclear and near-infrared fluorescence imaging show comparable detection sensitivity. With regard to quantification, nuclear techniques are superior to fluorescence imaging. Regarding the latter, alternatively fluorescence resonance energy transfer (FRET) technique has been employed and drug release can be real time reflected via the recovered fluorescence.[20] However, efficient FRET between DDS (the donor) and drug (the acceptor) requires the DDS and drug to possess well spectral overlapping and keep a rational distance (typically less than 10 nm) simultaneously,[21] which make the preparation process arduous. Therefore, construction of easy-to-fabricated drug delivery systems with real-time monitoring of drug release is still highly challenging and desirable.

To address the aforementioned issues, we fabricated a simple but rational nanoscale coordination polymer to deliver doxorubicin (DOX) to tumor region and real-time monitor of drug release. It is well documented that coordination polymers comprise well-ordered structures in which organic ligands and metal ions are connected by coordination bonds.[22,23] Herein, we chose Fe^{3+} as the metal ion and polyphenol gallic acid (GA) as the ligand. Thus the obtained coordination polymer is designated as FGC. As shown in **Figure 1**, FGC could form polygonal self-assembly, and GA as a natural polyphenol ingredient in green tea can inhibit tumor growth to some extent. Meanwhile, FGC could load DOX (denoted as FGC@DOX) with extremely high efficacy. Importantly, different from traditional
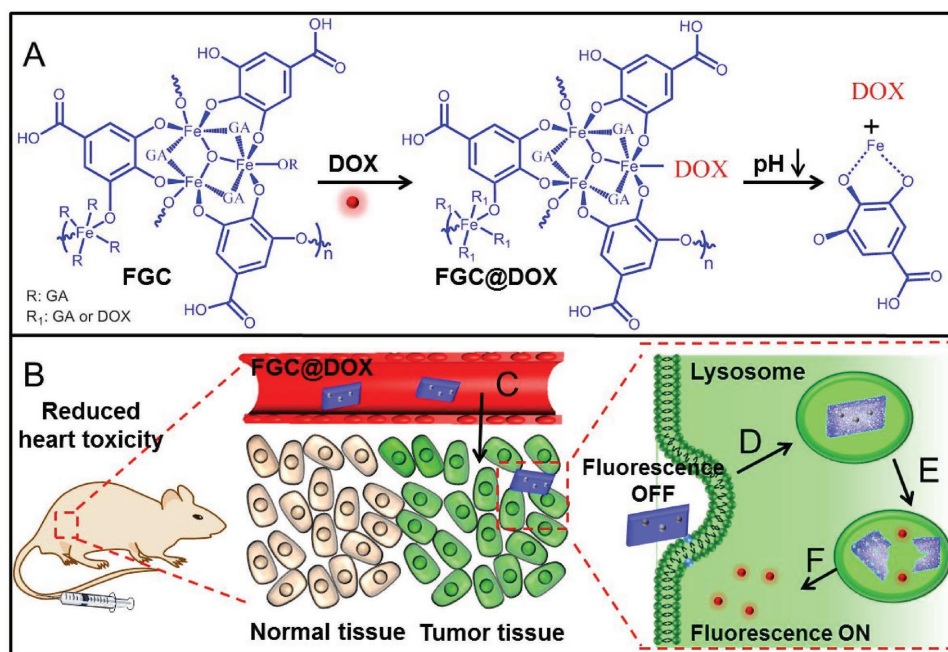
Figure 1. Schematic illustration of drug delivery system with monitored drug release: A) the mechanism of DOX loading on FGC and the acidic responsiveness; B) In vivo injection of fluorescence quenched FGC@DOX with reduced heart toxicity; C) EPR-induced tumor targeting; D) lysosome localization of FGC@DOX; E) the acidity-triggered degradation of FGC; and F) drug release and fluorescence recovery of DOX.

DDSs, the fluorescence of DOX kept quenched when DOX was conjugated with FGC at physiological environment. After internalized by tumor cells, DOX would be released in acidic lysosome and the fluorescence was gradually recovered. This "OFF-to-ON" switch in fluorescence of DOX realized real-time monitoring of drug release. Furthermore, nanoscale FGC@DOX could target tumor tissue via enhanced penetration and retention (EPR) effect,[24,25] and exhibited improved antitumor effect with minimal heart toxicity in vivo using a nude mice model.

2. Results and Discussion

2.1. Synthesis and Characterizations of FGC and FGC@DOX

FGC was fabricated via a microwave-assisted heating method. Transmission electron microscope (TEM) image revealed that well-dispersed and regular polygon nanoparticles would form in water (**Figure 2**A). Absorption spectra of iron(III) gallates gave evidence of formation of *bis*- and *tris*-complexes (Figure S1, Supporting Information). The dd bands of the corresponding iron(III) complexes have the maximum at 559 nm for 2:1 complexes and 472 nm for 3:1 complexes.[26] Subsequently, DOX was mixed with FGC, and free DOX was removed by repeated washing and centrifugation to get FGC@DOX. Figure 2B suggested that encapsulation of DOX did not significantly affect the morphology of FGC. The dynamic light scattering result showed that hydrodynamic sizes of FGC and FGC@DOX were 417 ± 11 and 482 ± 16 nm, respectively (Figure S2, Supporting Information). The hydrodynamic size was larger than that observed via TEM, since

TEM was observed under vacuum and samples would be shrinkage.[27] Encapsulation of DOX by FGC was mainly due to the coordination interaction between Fe^{3+} centers and deprotonated hydroxyl groups of the aglycone moiety in DOX.[28] It was also confirmed by X-ray photoelectron spectrum (XPS). As shown in Figure 2C, Fe $2p_{1/2}$ and Fe $2p_{3/2}$ peaks appeared at 725.2 and 711.7 eV, respectively. A separation of 13.5 eV between Fe $2p_{1/2}$ and Fe $2p_{3/2}$ peaks indicated the presence of trivalent state iron. Meanwhile, the auger chemical shift (3.5 eV) compared with the binding energy of $Fe(NO_3)_3$ suggested that Fe^{3+} was coordinated with DOX. And this result was consistence with the previous report.[29] Moreover, the UV–vis spectrum verified that the absorption band of DOX slightly shifted to the red, and typical absorbance shoulder peaks between 600 and 700 nm appeared for FGC@DOX (Figure 2D), which further substantially demonstrated the coordination interaction between Fe^{3+} and DOX.[28] In addition, it was found that FGC was negatively charged, whose ξ potential was around −25 mV (Figure 2E) due to the fact that FGC was composed of Fe^{3+} and negatively charged GA. The ξ potential significantly increased to around −8 mV, when DOX was loaded, since the coordination of DOX introduced positively charged free amines. Thermal gravimetric analysis (TGA) curves revealed that the weight loss values of FGC and FGC@DOX were 55.0% and 83.6%, respectively, when temperature increased to 400 °C (Figure 2F). The increased weight loss of FGC@DOX indicated that DOX was successfully loaded onto FGC. Besides, it was found that the infrared peaks of benzene ring (1532 and 1365 cm^{-1}) were observed in FGC, and the new peaks at 1647 (νRing) and 2923 cm^{-1} (νC−H) appeared in FGC@DOX, suggesting the existence of DOX (Figure S3, Supporting Information).

ADVANCED
SCIENCE NEWS
www.advancedsciencenews.com

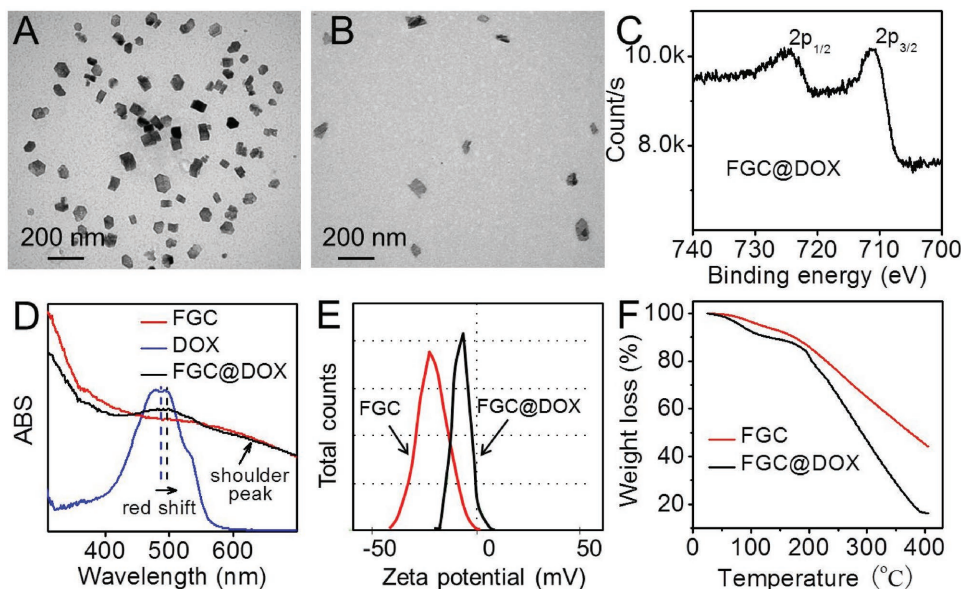ADVANCED
HEALTHCARE
MATERIALS
www.advhealthmat.de

Figure 2. TEM images of A) FGC and B) FGC@DOX. C) The XPS spectrum of FGC@DOX. D) The UV–vis spectrum of FGC, DOX, and FGC@DOX. E) The ξ potential of FGC and FGC@DOX. F) Thermal gravimetric analysis of FGC and FGC@DOX.

2.2. Drug Loading and Release in FGC@DOX

DOX loading efficiency by FGC was determined via the UV–vis spectrum. Surprisingly, the loading efficiency was as high as 48.3%, and the drug loading content (about 93.5%) was also extremely high, which meant 93.5 µg of DOX per 100 µg of FGC support. Meanwhile, FGC@DOX has well stability; the change in hydrodynamic size was negligible with prolonging of storage time (Figure S4, Supporting Information). Undoubtedly, FGC@DOX presented dramatically increased drug loading efficiency, when compared with the conventional drug encapsulation approach and the drug–polymer conjugation method whose typical drug loading efficiencies are less than 5% and 10%, respectively.[30] This high loading efficiency was due to the sufficient Fe^{3+} centers, which provided a great of coordination interaction sites with DOX. Meanwhile, FGC as a nanoscale coordination polymer was not so compact, which further benefited the coordination interaction.

It is worth mentioning that the fluorescence of DOX would be quenched when DOX was loaded on FGC. As shown in **Figure 3**A, a progressive decrease in fluorescence intensity was observed with increasing the concentration of FGC. This decreased fluorescence was due to the formation of nonemissive ground-state complexes.[28,31] Since both −OH−Fe^{3+} bonds in FGC and the coordination interaction between FGC and DOX were fairly stable under neutral condition, but prone to be attacked by mild acids,[32–34] so DOX was expected to be

released from FGC@DOX under acidity, leading to pH-responsive fluorescence recovery. To confirm it, the fluorescence spectrum of FGC@DOX at pHs of 5.0 and 7.4 at different times was recorded. As shown in Figure 3B, fluorescence of DOX increased dramatically with time prolonging, when FGC@DOX was incubated in phosphate buffer solution (PBS) at pH 5.0. On the contrary, the fluorescence increasing rate was significantly
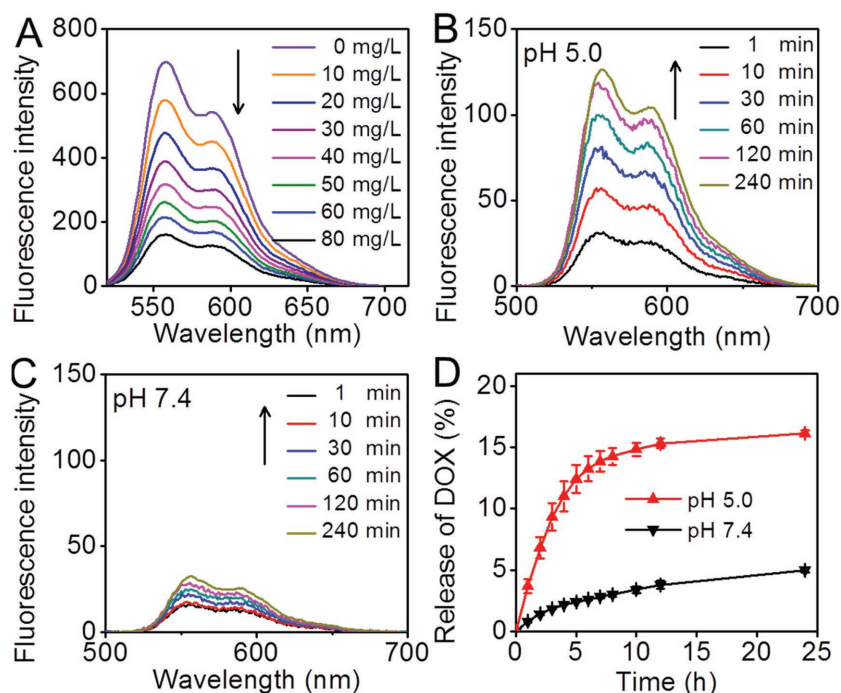

Figure 3. A) Fluorescence quenching of DOX by FGC, the concentration of DOX was 20 mg L^{-1}. Fluorescence recovery of DOX in FGC@DOX at B) pH 5.0 and C) pH 7.4. D) Drug release curves at pHs 5.0 and 7.4.

ADVANCED
SCIENCE NEWS
www.advancedsciencenews.com

ADVANCED
HEALTHCARE
MATERIALS
www.advhealthmat.de

retarded at pH 7.4 (Figure 3C). As expected, mild acidity liberated DOX and realized fluorescence recovery. Meanwhile, the drug release curves in vitro revealed that FGC@DOX exhibited a pH-controlled drug release behavior (Figure 3D). At the initial stage of drug release (less than 8 h), the release amount of DOX at pH 5.0 was above fivefolds to that at pH 7.4. And the drug release amount at pH 5.0 was 16.2% at the 24th hour, which was significantly higher than that at pH 7.4 (around 5%). Similar result was also reported previously.[31] It was due to that only a part of $-OH-Fe^{3+}$ bonds were hydrolyzed in FGC, which restricted the drug release. And this could be reflected by TEM that the morphology of FGC did not significantly change (Figure S5, Supporting Information).

2.3. Cellular Localization, Monitoring of Drug Release, and Cytotoxicity In Vitro

Encouraged by the pH-responsive drug release and fluorescence recovery, we further explored the feasibility of FGC@DOX in monitoring the drug release inside tumor cells. Before that, the cellular localization of FGC@DOX in human cervical carcinoma (HeLa) cells was studied via confocal laser scanning microscope (CLSM). FGC@DOX was incubated with HeLa cells for 4 h for cellular internalization. Thereafter, the medium was replaced and cells were further incubated for 3 h. Acidic subcellular organelle lysosome was labeled with LysoTracker Green. As shown in **Figure 4**A, the green fluorescence was overlapped well with red fluorescence, indicating that FGC@DOX was mainly entrapped in lysosome. Meanwhile, the acids in lysosome hydrolyzed FGC@DOX, realizing the fluorescence recovery of DOX.

Subsequently, the real-time release of DOX from FGC@DOX in lysosome at preset times was observed via CLSM after FGC@DOX was internalized by HeLa cells. As shown in Figure 4B, red fluorescence was very weak at 0 h, since the release of DOX was time dependent and fluorescence of DOX still kept quenched at the initial stage of entrapment in lysosome. With prolonging of incubation time from 0 to 1.5 and 4.5 h, the red signal of DOX observably increased. Clearly, DOX was gradually released in lysosome. Meanwhile, the release

amount at various time points could be directly reflected by the intensity of recovered fluorescence; in other words, DOX release in HeLa cells could be real-time monitored. After DOX was released, due to the existence of various enzymes and the acidic environment, the coordination polymer was expected to gradually degrade in digestive lysosome with enough time.

After DOX was released in cells, it was expected to combine with DNA and inhibit cell growth. To evaluate the cytotoxicity of FGC@DOX, 3-[4,5-dimethylthiazol-2-yl]-2,5-diphenyltetrazolium-bromide (MTT) assay was employed, and FGC and DOX were used as controls. As shown in Figure 4C, FGC exhibited significant toxicity to HeLa cells due to the presence of natural antioxidant GA.[35] Obviously, FGC acted not only as the drug carrier but also as the effective therapeutic biosubstance. Meanwhile, FGC@DOX exhibited remarkably higher toxicity to HeLa cells than that of FGC. This result was attributed to the high efficient DOX encapsulation as well as the inherent therapeutic effect of FGC. We also noticed that the toxicity of FGC@DOX was lower than that of free DOX, especially at the high concentration of DOX. It was due to the fact that release of DOX from FGC@DOX was time consuming.[36]

2.4. In Vivo Biodistribution and Antitumor Effect of FGC@DOX

Motivated by well inhibition of tumor cells in vitro, we proceeded to perform the in vivo tests by assessing biodistribution and antitumor effect of FGC@DOX on female nude mice. As shown in **Figure 5**A, the fluorescence of free DOX was distributed in almost whole body. In sharp contrast, a strong fluorescence signal was observed in the tumor region in FGC@DOX-treated mouse, while the signal in other regions was remarkably decreased. These results suggested that nanoscale FGC@DOX could target to tumor tissue via EPR effect. Subsequently, in vivo antitumor therapy of FGC@DOX via intravenous injection was evaluated. PBS, FGC, and DOX were employed as the controls. As shown in Figure 5B, FGC could retard tumor growth to some extent, which was consistence with the cytotoxicity result in vitro. Meanwhile, as a widely used antitumor drug, DOX could significantly inhibit tumor growth. Importantly, FGC@DOX almost retarded tumor growth
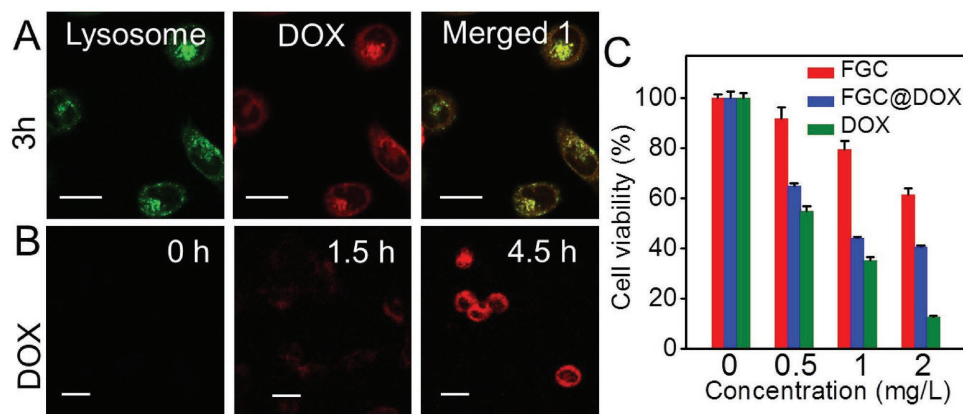

Figure 4. A) Lysosome localization of FGC@DOX in HeLa cells. Red signal: DOX; green signal: LysoTrakcer Green. B) Fluorescence recovery of DOX at different times: 0, 1.5, and 4.5 h. The scale bar was 20 µm. C) Cytotoxicity in vitro of DOX, FGC, and FGC@DOX against HeLa cells.
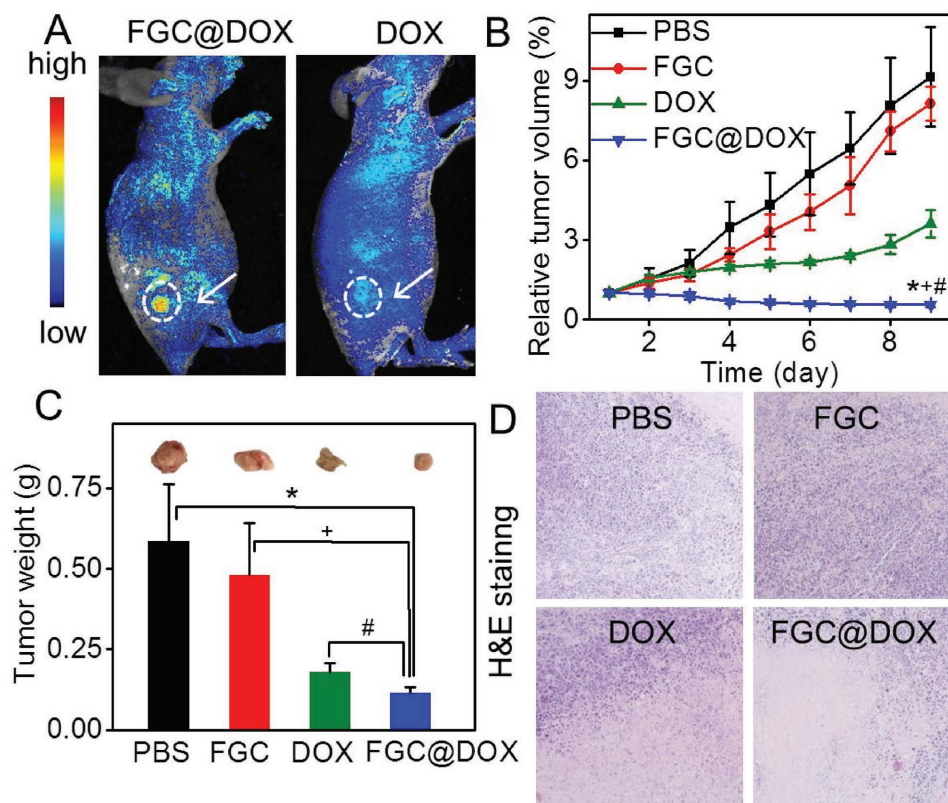
**ADVANCED
SCIENCE NEWS**
www.advancedsciencenews.com

**ADVANCED
HEALTHCARE
MATERIALS**
www.advhealthmat.de

Figure 5. A) In vivo imaging of FGC@DOX- and DOX-treated mouse, with the white arrow pointing to the tumor tissue. The blue channel was chosen for imaging. In vivo antitumor efficacy: B) relative tumor volume; C) average tumor weight (inset was the representative tumor image of various groups); D) histological observation of tumor tissues (×40) via H&E staining. *p, +p, #p < 0.01 was tested via a Student's t-test when the group of FGC@DOX was compared with other groups.

completely, and the tumor growth inhibition ability was even better than DOX. Clearly, the in vivo antitumor results between FGC@DOX and DOX were different from that of cytotoxicity in vitro. This substantial discrepancy was due to following issues: antitumor therapy in vivo was a relatively long-term process, when compared with cytotoxicity in vitro. FGC@DOX had enough time to release DOX in the tumor region in a controlled manner, which optimized the tumor inhibition efficacy of DOX and realized the synergic effect between FGC and DOX. However, DOX would not target and accumulate in tumor region, which dramatically compromised the antitumor effect. These antitumor results were further supported by the tumor weight, representative tumor image (Figure 5C) as well as hematoxylin and eosin (H&E) staining. As shown in Figure 5D, tumor cells in PBS group were dense and compact. And the cell density was gradually deceased in the following order: PBS > FGC > DOX > FGC@DOX. Mice treated with FGC@DOX exhibited the absence of furthest nuclei in tumor tissue, suggesting the death of most tumor cells.

2.5. In Vivo Systemic Toxicity Evaluation of FGC@DOX

An ideal drug delivery system should possess both well antitumor effect and negligible side effects. To evaluate the potential side effects during in vivo therapy, the body weight of mice

was recorded. As shown in **Figure 6**A, the body weight in PBS, FGC, and FGC@DOX were relatively stable, indicating the low systemic side effects. In contrast, the body weight in the DOX group significantly decreased with the prolonging of therapeutic time, suggesting the appearance of acute drug toxicity.[37] At the 9th day, the first mouse in the DOX group was dead, and the treatment was finished. Then mice were further fed and survival rate was recorded. As shown in Figure 6B, at the 12th day, the second mouse in the DOX group was dead. Meanwhile, no mice were dead in other groups. Clearly, although DOX could significantly inhibit tumor growth, it also presented great undesired side effects which even killed mouse itself. These side effects were due to the systematic distribution of DOX after tail intravenous injection. And these results were also consistence with previous reports.[38,39]

To further demonstrate the potential mechanism of side effects, the serum samples of various groups were collected after the mice were sacrificed. A series of physiological and biochemical indices about liver, kidneys, and heart were recorded. It was found that there did not exist significant differences in the expression level of liver functional biomarkers in terms of glutamic pyruvate transaminase (GPT; Figure 6C) and aspartate aminotransferase (AST; Figure 6D), kidney functional biomarkers in terms of blood urea nitrogen (BUN; Figure 6E), and uric acid (UA; Figure 6F) among various groups. However, the expression level of heart functional biomarker creatinine
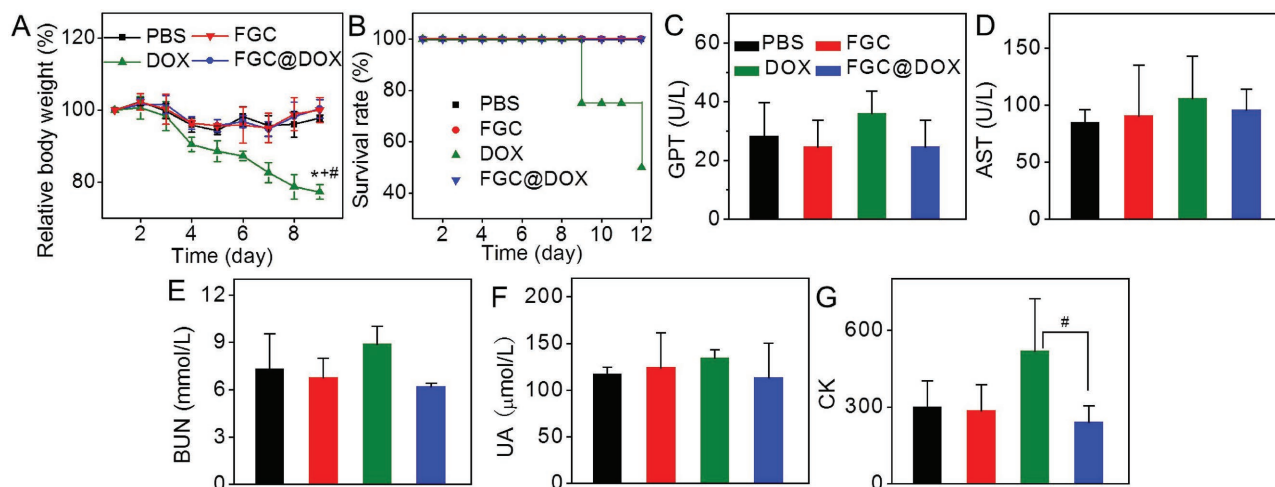
Figure 6. A) Relative body weight and B) mice survival rate during treatment. $*p$, $+p$, $\#p < 0.01$ was tested via a Student's t-test, when the group of FGC@DOX was compared with other groups. Blood routine analysis of various groups after 9 d treatment: C) GPT; D) AST; E) BUN; F) UA, and G) CK. $\#p < 0.01$ was tested via a Student's t-test when the group of FGC@DOX was compared with the group of DOX.

phosphkinase (CK) in the DOX group was significantly higher than other groups (Figure 6G). Obviously, although DOX did not damage liver and kidneys, it presented severe heart toxicity. On the contrary, despite the high content of DOX in FGC@DOX, the side effects of FGC@DOX were still negligible. This difference was mainly attributed to the following factors: FGC@DOX was relative stable at pH 7.4, which could avoid to the leakage of DOX during circulation furthest. Certainly, a little DOX would be released into blood from FGC@DOX inevitably with prolonging of circulation time. However, tissues were continuously exposed to a low-dose drug

environment, which could efficiently avoid high peak level of DOX as well as the acute toxicity.[40] On the other hand, the existence of natural polyphenol GA could protect cardiomyocytes from DOX-induced heart damage.[41–43] Meanwhile, the tumor targeting capability of FGC@DOX in vivo also restricted the toxicity of DOX in tumor.

In addition, the histological morphology of heart, lung, spleen, liver, and kidneys was also conducted via hematoxylin and eosin (H&E) staining to observe the organ damage directly. As shown in **Figure 7**, for the DOX group, the kidney and liver sections appeared normal. However, the myocytes significantly
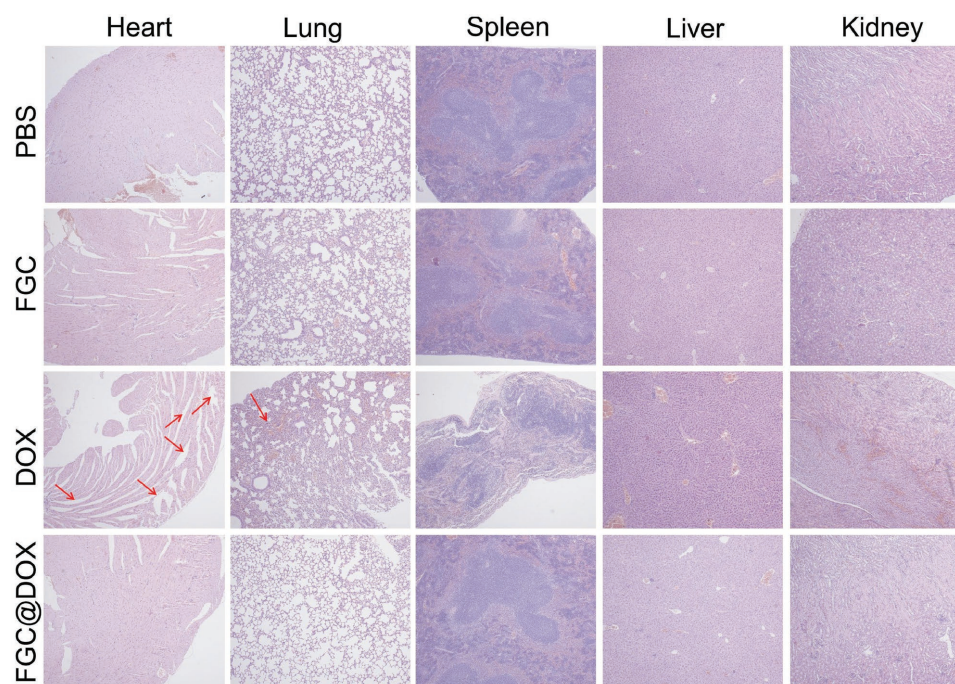

Figure 7. Representative histological sections of light microscopy of heart (×40), lung (×40), spleen (×40), liver (×40), and kidney (×40) tissue sections by H&E staining. The red arrow pointed to the damaged region.

**ADVANCED
SCIENCE NEWS**

www.advancedsciencenews.com

**ADVANCED
HEALTHCARE
MATERIALS**

www.advhealthmat.de

dissolved in heart while the alveolar walls became thicken, which substantially indicated the damage of DOX to heart and lung.[44] On the contrary, negligible pathological changes were found in PBS, FGC, and FGC@DOX groups in these organs. Taken together, the self-delivery system FGC@DOX presented novel antitumor effect with minimal side effects in vivo.

3. Conclusion

In summary, we developed a nanoscale FGC@DOX drug delivery system with pH-responsive monitoring of drug release for enhanced tumor therapy and minimal side effects. FGC possessed extremely high drug loading and fluorescence quenching capability simultaneously. Meanwhile, DOX could be released in acidic organelle lysosome. And this process would be real-time monitored by recovered fluorescence of DOX. Besides, this polyphenol-rich FGC@DOX drug delivery system inhibited tumor growth significantly with minimal heart toxicity in vivo due to the tumor target ability, controlled drug release, as well as the presence of polyphenol in FGC@DOX. The coordination polymer demonstrated here addressed the bottlenecks of traditional DDSs, i.e., disappointed drug loading capability, unknown drug release, as well as significant side effects, which should open a window in the design of drug delivery systems.

4. Experimental Section

Chemicals: GA was purchased from Aladdin Reagent Co. Ltd. (Shanghai, China). Iron(II) chloride tetrahydrate ($FeCl_2 \cdot 4H_2O$) were obtained from Shanghai Chemical Co. (Shanghai, China). Dulbecco's modified Eagle's medium (DMEM), trypsin, fetal bovine serum, MTT, penicillin–streptomycin were provided by GIBCO Invitrogen Corp. All other materials were used without further purification.

Synthesis of FGC: FGC was prepared via the microwave-assisted heating method. Briefly, 0.199 g of $FeCl_2 \cdot 4H_2O$ (0.001 mol) and 0.170 g of gallic acid (0.001 mol) were dissolved in 20 mL dimethyl formamide (DMF).[45] The solution was placed in a microwave vessel, and mixture was then rapidly heated to 156 °C. The reaction maintained for 8 h and then the solution was cooled to room temperature. FGC was isolated by high-speed centrifugation and further purified by repeatedly washing with ethanol and water successively. FGC was dispersed in water for further use.

DOX Loading and Release Study: About 2.0 mg of FGC was mixed with 3 mg of DOX in 10.0 mL water and stirred at room temperature overnight. Then mixture was centrifuged at 8000 rpm and washed with PBS (pH 7.4) repeatedly until the supernatant solution had no fluorescent signal of DOX. The obtained FGC@DOX was dispersed in water for further use. To determine the loading amount of DOX, all the supernatant solutions containing with DOX were collected. The amount of DOX in these supernatants was measured by a UV–vis spectrophotometer (absorption at 480 nm). The loading amount of DOX was calculated as (mass of DOX fed initially − mass of DOX in supernatant solution). Drug loading efficiency (DLE) was defined as DLE = mass of DOX loaded in FGC/mass of FGC@DOX × 100%. Drug loading content (DLC) was defined as DLC = mass of DOX loaded in FGC/mass of FGC × 100%.[46]

For a drug release study, 0.4 mg of FGC@DOX was dispersed in 4 mL of PBS buffer at pHs of 7.4 and 5.0, respectively. Then the solution was positioned to a dialysis bag (molar weight cut-off: 1000 Da) and dialyzed against corresponding PBS buffer. The dialysis solution was collected at preset time and fresh PBS buffer was added. The concentration of released DOX was measured by the fluorescence spectrum.

Characterization of FGC and FGC@DOX: The hydrodynamic size of FGC (50 mg L^{-1}) and FGC@DOX (50 mg L^{-1}) were determined via Zetasizer Nano-ZS (Malvern Instruments Ltd). To test the stability, FGC@DOX was dispersed in water and the sizes at the second and fourth hour were determined. The samples in KBr pellets were analyzed by a Spectrum Two Fourier Transform Infrared spectrophotometer (Perkin Elmer). Morphologies of FGC (50 mg L^{-1}) and FGC@DOX were observed by TEM (JEM-2100 microscope). FGC was incubated in acidic water (pH 5) for 4 h and then observed via TEM to test if it could disassemble. ξ potentials of FGC and FGC@DOX (20 mg L^{-1}) were determined through Zetasizer Nano-ZS (Malvern Instruments Ltd). The UV–vis spectrum of FGC, DOX, and FGC@DOX was determined via the UV–vis spectrophotometer (Perkin Elmer). XPS analysis was conducted via an X-ray photoelectron spectrometer (ESCALAB 250Xi, Thermo Fisher). TGA was conducted on a TGS2 thermogravimetric analyzer (Perkin Elmer).

Fluorescence Quenching and pH-Responsive Fluorescence Recovery: For fluorescence quenching study, various concentrations of FGC solutions were added to DOX solution (20 mg L^{-1}), and the fluorescence spectrum of DOX was determined immediately. For pH responsive fluorescence recovery, FGC@DOX (20 mg L^{-1}) was incubated in PBS buffer at pHs of 7.4 and 5.0, respectively. The fluorescence spectrum of DOX was recorded at preset time.

Cytotoxicity In Vitro: The in vitro cytotoxicity against HeLa cells was studied via MTT assay. Briefly, HeLa cells were seeded on 96-well plates (6000 cells each well). After 24 h, various concentrations of FGC@DOX, DOX, and FGC solution were added to 96-well plates, respectively. After incubation for 48 h, 20 μL MTT solution (5 mg mL^{-1}) was added to each well. And 4 h later, the supernatant was replaced with dimethylsulfoxide (150 μL). The optical density (OD) at 570 nm was recorded via a microplate reader (Bio-Rad, Model 550, USA). The cell viability was calculated as following: cell viability (%) = OD$_{(sample)}$/OD$_{(control)}$ × 100%. OD$_{(sample)}$ was the OD value in the presence of the sample, and OD$_{(control)}$ was the OD value in the absence of the sample.

Fluorescence Recovery and Cellular Localization In Vitro: For fluorescence recovery study, HeLa cells were seeded on the 6-well plate (1×10^5 cells per well). After incubated at 37 °C for 24 h, FGC@DOX was added to 6-well plates, and cells were incubated for 4 h. Then sample was replaced with fresh medium and the cells were further incubated for 0, 1.5, and 4.5 h, respectively. Subsequently, cells were washed with PBS three times and observed directly via CLSM (C1-Si, Nikon, Japan). For the cellular localization study, FGC@DOX was incubated with HeLa cells for 4 h, and then the medium was replaced with fresh medium. Cells were further incubated for 3 h. Thereafter, the lysosome was stained with 20 μL LysoTracker Green (2 mg mL^{-1}) at 37 °C for 30 min. Then cells were repeatedly washed with PBS and incubated with 500 μL DMEM for further CLSM observation.

In Vivo Biodistribution Study: Animal experiments were approved by the Scientific Ethic Committee of Huazhong Agricultural University (HZAUMO-2016-044) and conducted based on the guidelines for laboratoy animals established by Huazhong Agricultural University. To establish the H22 tumor-bearing mouse model, ascites containing H22 cells were collected from the peritoneal cavity of the BALB/c mouse after 6 d. Then 100 μL of the ascites containing H22 cells (5×10^6 cells per mouse) were injected into the back of nude mice subcutaneously to get tumor-bearing mouse model. When the tumor size was around 200 mm^3, mice were injected with FGC@DOX and DOX via the tail vein, respectively. The dosage of DOX was 3 mg kg^{-1} per mouse. At the 2 h post of in vivo injection, mice were anesthetized and imaged via a small animal imaging system.

In Vivo Antitumor Efficacy: About 100 μL of H22 cells (5×10^6 cells per mouse) was injected into the back of mice subcutaneously. After 2 d, the mice size would be around 50 mm^3; mice were divided into four groups randomly and injected with PBS, DOX, FGC, and FGC@DOX via the tail vein, respectively. Each group had four mice. The dosage of DOX was 3 mg kg^{-1} per mouse. Injection was given every day. The body weight and tumor volume were measured immediately before injection. Tumor volume was calculated as $V = W^2 \times L/2$ where W and L were the shortest and longest diameters of tumor, respectively. The relative tumor volume

**ADVANCED
SCIENCE NEWS**

www.advancedsciencenews.com

**ADVANCED
HEALTHCARE
MATERIALS**

www.advhealthmat.de

was calculated as volume of the tumor at the point of measurement (V_t)/volume of the tumor at the first day of treatment (V_0). After the treatment finished, mice were executed and weights of all tumors were recorded.

Systemic Toxicity In Vivo: Before the mice were executed, the blood sample of mice in various groups was collected. The blood was solidified and the supernatant serum was collected. The content of GPT, AST, BUN, UA, CK in serum samples was detected in Wuhan Union Hospital. Besides, after the mice were executed, tissues of various groups including heart, liver, lung, spleen, kidneys, and tumor were exfoliated and collected. The tissue morphology was observed via H&E staining.

Statistical Analysis: Statistical analysis was performed using a Student's *t*-test. The differences were considered to be statistically significant for a *p*-value of <0.05.

Supporting Information

Supporting Information is available from the Wiley Online Library or from the author.

Conflict of Interest

The authors declare no conflict of interest.

[1] Y. Matsumoto, J. W. Nichols, K. Toh, T. Nomoto, H. Cabral, Y. Miura, R. J. Christie, N. Yamada, T. Ogura, M. R. Kano, Y. Matsumura, N. Nishiyama, T. Yamasoba, Y. H. Bae, K. Kataoka, *Nat. Nanotechnol.* **2016**, *11*, 533.

[2] R. Xu, G. D. Zhang, J. H. Mai, X. Y. Deng, V. Segura-Ibarra, S. H. Wu, J. L. Shen, H. R. Liu, Z. H. Hu, L. X. Chen, Y. Huang, E. Koay, Y. Huang, J. Liu, J. E. Ensor, E. Blanco, X. W. Liu, M. Ferrari, H. F. Shen, *Nat. Biotechnol.* **2016**, *34*, 414.

[3] Y. M. Zhao, F. Fay, S. Hak, J. M. Perez-Aguilar, B. L. Sanchez-Gaytan, B. Goode, R. Duivenvoorden, C. L. Davies, A. Bjørkøy, H. Weinstein, Z. A. Fayad, C. Pérez-Medina, W. J. M. Mulder, *Nat. Commun.* **2016**, *7*, 11221.

[4] X. Z. Ai, C. J. H. Ho, J. X. Aw, A. B. E. Attia, J. Mu, Y. Wang, X. Y. Wang, Y. Wang, X. G. Liu, H. B. Chen, M. Y. Gao, X. Y. Chen, E. K. L. Yeow, G. Liu, M. Olivo, B. G. Xing, *Nat. Commun.* **2016**, *7*, 10432.

[5] J. E. Chung, S. Tan, S. J. Gao, N. Yongvongsoontorn, S. H. Kim, J. H. Lee, H. S. Choi, H. Yano, L. Zhuo, M. Kurisawa, J. Y. Ying, *Nat. Nanotechnol.* **2014**, *9*, 907.

[6] K. Cai, X. He, Z. Song, Q. Yin, Y. Zhang, F. M. Uckun, C. Jiang, J. Cheng, *J. Am. Chem. Soc.* **2015**, *137*, 3458.

[7] K. Han, Q. Lei, H. Z. Jia, S. B. Wang, W. N. Yin, W. H. Chen, S. X. Cheng, X. Z. Zhang, *Adv. Funct. Mater.* **2015**, *25*, 1248.

[8] J. A. Floyd, A. Galperin, B. D. Ratner, *Adv. Drug Delivery Rev.* **2015**, *91*, 23.

[9] S. Merino, C. Martín, K. Kostarelos, M. Prato, E. Vázquez, *ACS Nano* **2015**, *9*, 4686.

[10] J. F. Zhang, Y. C. Liang, X. D. Lin, X. Y. Zhu, L. Yan, S. L. Li, X. Yang, G. Y. Zhu, A. L. Rogach, P. K. N. Yu, P. Shi, L. C. Tu, C. C. Chang, X. H. Zhang, X. F. Chen, W. J. Zhang, C. S. Lee, *ACS Nano* **2015**, *9*, 9741.

[11] S. Y. Qin, A. Q. Zhang, S. X. Cheng, L. Rong, X. Z. Zhang, *Biomaterials* **2017**, *112*, 234.

[12] K. Han, Q. Lei, S. B. Wang, J. J. Hu, W. X. Qiu, J. Y. Zhu, W. N. Yin, X. Luo, X. Z. Zhang, *Adv. Funct. Mater.* **2015**, *25*, 2961.

[13] P. Huang, D. L. Wang, Y. Su, W. Huang, Y. F. Zhou, X. Y. Zhu, D. Y. Yan, *J. Am. Chem. Soc.* **2014**, *136*, 11748.

[14] H. Kasai, T. Murakami, Y. Ikuta, Y. Koseki, K. Baba, H. Oikawa, H. Nakanishi, M. Okada, M. Shoji, M. Ueda, H. Imahori, M. Hashida, *Angew. Chem. Int. Ed.* **2012**, *51*, 10315.

[15] J. Tang, B. Kong, H. Wu, M. Xu, Y. C. Wang, Y. L. Wang, D. Y. Zhao, G. F. Zheng, *Adv. Mater.* **2013**, *25*, 6569.

[16] J. N. Liu, J. W. Bu, W. B. Bu, S. J. Zhang, L. M. Pan, W. P. Fan, F. Chen, L. P. Zhou, W. J. Peng, K. L. Zhao, J. L. Du, J. L. Shi, *Angew. Chem., Int. Ed.* **2014**, *53*, 4551.

[17] J. Zhang, Z. F. Yuan, Y. Wang, W. H. Chen, G. F. Luo, S. X. Cheng, R. X. Zhuo, X. Z. Zhang, *J. Am. Chem. Soc.* **2013**, *135*, 5068.

[18] K. Pant, O. Sedláček, R. A. Nadar, M. Hrubý, H. Stephan, *Adv. Healthcare Mater.* **2017**, *6*, 1601115.

[19] S. Santra, C. Kaittanis, O. J. Santiesteban, J. M. Perez, *J. Am. Chem. Soc.* **2011**, *133*, 16680.

[20] J. P. Lai, B. P. Shah, E. Garfunkel, K. B. Lee, *ACS Nano* **2013**, *7*, 2741.

[21] S. Y. Li, H. Cheng, B. R. Xie, W. X. Qiu, L. L. Song, R. X. Zhuo, X. Z. Zhang, *Biomaterials* **2016**, *104*, 297.

[22] M. Guardingo, P. González-Monje, F. Novio, E. Bellido, F. Busqué, G. Molnár, A. Bousseksou, D. Ruiz-Molina, *ACS Nano* **2016**, *10*, 3206.

[23] Y. S. Yang, K. Z. Wang, D. P. Yan, *ACS Appl. Mater. Interfaces* **2016**, *8*, 15489.

[24] Y. Matsumura, H. Maeda, *Cancer Res.* **1986**, *46*, 6387.

[25] A. K. Iyer, G. Khaled, J. Fang, H. Maeda, *Drug Discovery Today* **2006**, *11*, 812.

[26] A. Ghadban, A. S. Ahmed, Y. Ping, R. Ramos, N. Arfin, B. Cantaert, R. V. Ramanujan, A. Miserez, *Chem. Commun.* **2016**, *52*, 697.

[27] W. Tao, J. X. Zhang, X. W. Zeng, D. Liu, G. Liu, X. Zhu, Y. L. Liu, Q. T. Yu, L. Q. Huang, L. Mei, *Adv. Healthcare Mater.* **2015**, *4*, 1203.

[28] R. Anand, F. Borghi, F. Manoli, I. Manet, V. Agostoni, P. Reschiglian, R. Gref, S. Monti, *J. Phys. Chem. B* **2014**, *118*, 8532.

[29] Y. J. He, L. Xing, P. F. Cui, J. L. Zhang, Y. Zhu, J. B. Qiao, J. Y. Lyu, M. Zhang, C. Q. Luo, Y. X. Zhou, N. Lu, H. L. Jiang, *Biomaterials* **2017**, *113*, 266.

[30] R. Duncan, *Nat. Rev. Cancer* **2006**, *6*, 688.

[31] W. J. Fang, J. Yang, J. W. Gong, N. F. Zheng, *Adv. Funct. Mater.* **2012**, *22*, 842.

[32] J. J. Richardson, M. Björnmalm, F. Caruso, *Science* **2015**, *348*, 2491.

[33] H. Ejima, J. J. Richardson, K. Liang, J. P. Best, M. P. van Koeverden, G. K. Such, J. W. Cui, F. Caruso, *Science* **2013**, *341*, 154.

[34] J. L. Guo, Y. Ping, H. Ejima, K. Alt, M. Meissner, J. J. Rich-ardson, Y. Yan, K. Peter, D. von Elverfeldt, C. E. Hagemeyer, F. Caruso, *Angew. Chem. Int. Ed.* **2014**, *53*, 5546.

[35] J. P. Perchellet, H. U. Gali, E. M. Perchellet, D. S. Klish, A. D. Armbrust, *Basic Life Sci.* **1992**, *59*, 783.

[36] K. Han, S. Chen, W. H. Chen, Q. Lei, Y. Liu, R. X. Zhuo, X. Z. Zhang, *Biomaterials* **2013**, *34*, 4680.

[37] B. Liu, Y. Chen, C. Li, F. He, Z. Hou, S. S. Huang, H. M. Zhu, X. Y. Chen, J. Lin, *Adv. Funct. Mater.* **2015**, *25*, 4717.

[38] Y. Chen, K. L. Ai, J. H. Liu, G. Y. Sun, Q. Yin, L. H. Lu, *Biomaterials* **2015**, *60*, 111.

[39] G. Yu, W. Yu, L. Shao, Z. Zhang, X. Chi, Z. W. Mao, C. Y. Gao, F. H. Huang, *Adv. Funct. Mater.* **2016**, *26*, 8999.

[40] J. Yang, Y. Shimada, R. C. L. Olsthoorn, B. E. Snaar-Jagalska, H. P. Spaink, A. Kros, *ACS Nano* **2016**, *10*, 7428.

[41] E. Lecumberri, Y. M. Dupertuis, R. Miralbell, C. Pichard, *Clin. Nutr.* **2013**, *32*, 894.

[42] W. J. Li, S. P. Nie, M. Y. Xie, Y. Chen, C. Li, H. Zhang, *J. Agric. Food Chem.* **2010**, *58*, 8977.

[43] L. Ray, P. Kumar, K. C. Gupta, *Biomaterials* **2013**, *34*, 3064.

[44] X. R. Li, X. C. Yang, Z. Q. Lin, D. Wang, D. Mei, B. He, X. Y. Wang, X. Q. Wang, Q. Zhang, W. Gao, *Eur. J. Pharm. Sci.* **2015**, *76*, 95.

[45] R. K. Feller, A. K. Cheetham, *Solid State Sci.* **2006**, *8*, 1121.

[46] J. V. John, R. G. Thomas, H. R. Lee, H. Chen, Y. Y. Jeong, I. Kim, *Adv. Healthcare Mater.* **2016**, *5*, 1874.

1700470 (9 of 9)